Nanoscale

Surface band bending and carrier dynamics in colloidal quantum dot solids

Journal:	*Nanoscale*
Manuscript ID	NR-ART-08-2021-005436.R2
Article Type:	Paper
Date Submitted by the Author:	08-Oct-2021
Complete List of Authors:	Clark, Pip; University of Manchester, Department of Physics and Astronomy and the Photon Science Institute Lewis, Nathan; University of Manchester, Department of Physics and Astronomy and the Photon Science Institute Ke, Chun-Ren; University of Manchester, Department of Physics and Astronomy and the Photon Science Institute Ahumada-Lazo, Rubén; University of Manchester, Department of Physics and Astronomy and the Photon Science Institute Chen, Qian; The University of Manchester, Department of Materials Neo, Darren; Institute of Materials Research and Engineering, advance optical technology Gaulding, Ashley; National Renewable Energy Laboratory, Pach, Gregory; National Renewable Energy Laboratory, Chemistry and Nanoscience Píš, Igor; IOM CNR, Laboratorio TASC Silly, Mathieu; Synchrotron SOLEIL, Flavell, Wendy; The University of Manchester, School of Physics

SCHOLARONE™
Manuscripts

Surface band bending and carrier dynamics in colloidal quantum dot solids

Pip C. J. Clark*[,a], Nathan K. Lewis[a], Jack Chun-Ren Ke[a], Ruben Ahumada-Lazo[a,‡], Qian Chen[b], Darren C. J. Neo[c,†], E. Ashley Gaulding[d], Gregory F. Pach[d], Igor Pis[e,f], Mathieu G. Silly[g], Wendy R. Flavell*[,a].

Band bending in colloidal quantum dot (CQD) solids has become important in driving charge carriers through devices. This is typically a result of band alignments at junctions in the device. Whether band bending is intrinsic to CQD solids, i.e. is band bending present at the surface-vacuum interface, has previously been unanswered. Here we use photoemission surface photovoltage measurements to show that depletion regions are present at the surface of n and p-type CQD solids with various ligand treatments (EDT, MPA, PbI_2, MAI/PbI_2). Using laser-pump photoemission-probe time-resolved measurements, we show that the timescale of carrier dynamics in the surface of CQD solids can vary over at least 6 orders of magnitude, with the fastest dynamics on the order of microseconds in PbS-MAI/PbI_2 solids and on the order of seconds for PbS-MPA and PbS-PbI_2. By investigating the surface chemistry of the solids, we find a correlation between the carrier dynamics timescales and the presence of oxygen contaminants, which we suggest are responsible for the slower dynamics due to deep trap formation.

1. Introduction

Colloidal quantum dots (CQDs) show a number of exciting properties such as tunability of photon absorption and emission, and efficient multiple exciton generation.[1,2] CQD solids, where CQDs are fabricated into a closely packed film, take on bulk material properties, as the wave functions of adjacent CQDs overlap,[3] coupling them together.[4] In CQD solids there is potential for controlling bulk properties, including the semiconductor doping level, carrier concentration, mobility, and lifetimes, through control of the CQD material, size, shape and surface chemistry.[4–10] This makes them applicable to a range of optoelectronic devices such as solar cells,[11,12] LEDs,[13] lasers,[14] and photodetectors.[15–17] Recently, control of the band alignment and band bending at junctions between CQD solids and oxides, metal cathodes or other CQD solids has become important for device design.[18–21] For example, in CQD photovoltaics this has led to more efficient carrier separation and extraction.[19,22–24] Still, the question remains: 'Is band bending intrinsic to CQD solids?' i.e., does band bending exist at the CQD solid-vacuum interface?

In conventional bulk semiconductors, surface band bending is a result of surface defects changing the electronic structure at the surface. In a CQD solid, each CQD has its own surface, and the CQDs at the surface of the solid should in principle be no different from those deeper in the bulk. The principle that CQD solids behave more like bulk semiconductors than individual quantum objects is established.[25–27] Properties such as dielectric constant and free carrier density can be treated by an effective-medium picture,[20] and it is well known that band bending occurs at solid junctions with CQD films.[28–30] Here, we explore whether band bending is present at the surface of CQD solids, by measuring the surface photovoltage (SPV) effect with photoemission.

The surface photovoltage effect is due to the separation of photoexcited electron-hole pairs in the surface band bending region of a semiconductor. The attraction between the separated electron and hole reduces the surface potential (amount of band bending). Figure 1 shows the creation and relaxation of a surface photovoltage shift in p- and n-type semiconductor surfaces. In the depletion region of an n-type semiconductor, a photoexcited electron migrates towards the bulk while the hole migrates to the surface, creating an SPV shift as shown in Figure 1. The SPV shift relaxes once all carriers have recombined and the surface potential is returned to its original value.[31] This can be measured with photoemission as either a change in the position of the valence band maximum (VBM), or, as implemented here, a change in the binding energy position of a core level peak.[32–34]

a. *Department of Physics and Astronomy and the Photon Science Institute, The University of Manchester, Manchester M13 9PL, United Kingdom.*
b. *Department of Materials, The University of Manchester, Manchester M13 9PL, United Kingdom.*
c. *Department of Chemistry, University of California, Irvine, Irvine, California 92697, United States.*
d. *National Renewable Energy Laboratory, Golden, CO 80401, USA.*
e. *Laboratorio TASC, IOM CNR, S.S. 14 km 163.5, 34149 Basovizza, Trieste, Italy.*
f. *Elettra-Sincrotrone Trieste S.C.p.A., S. S. 14 Km 163.5, 34149 Basovizza, Trieste, Italy.*
g. *Synchrotron SOLEIL, BP 48, Saint-Aubin, F91192 Gif sur Yvette CEDEX, France*
†Present address: Institute of Materials Research and Engineering (IMRE), 2 Fusionopolis Way, Innovis, #08-03, Singapore 13632.
‡Present address: Department of Physics, Durham University, Durham DH1 3LE, United Kingdom.
*Emails: pcjclark@gmail.com, wendy.flavell@manchester.ac.uk
Electronic Supplementary Information (ESI) available: [details of any supplementary information available should be included here]. See DOI: 10.1039/x0xx00000x
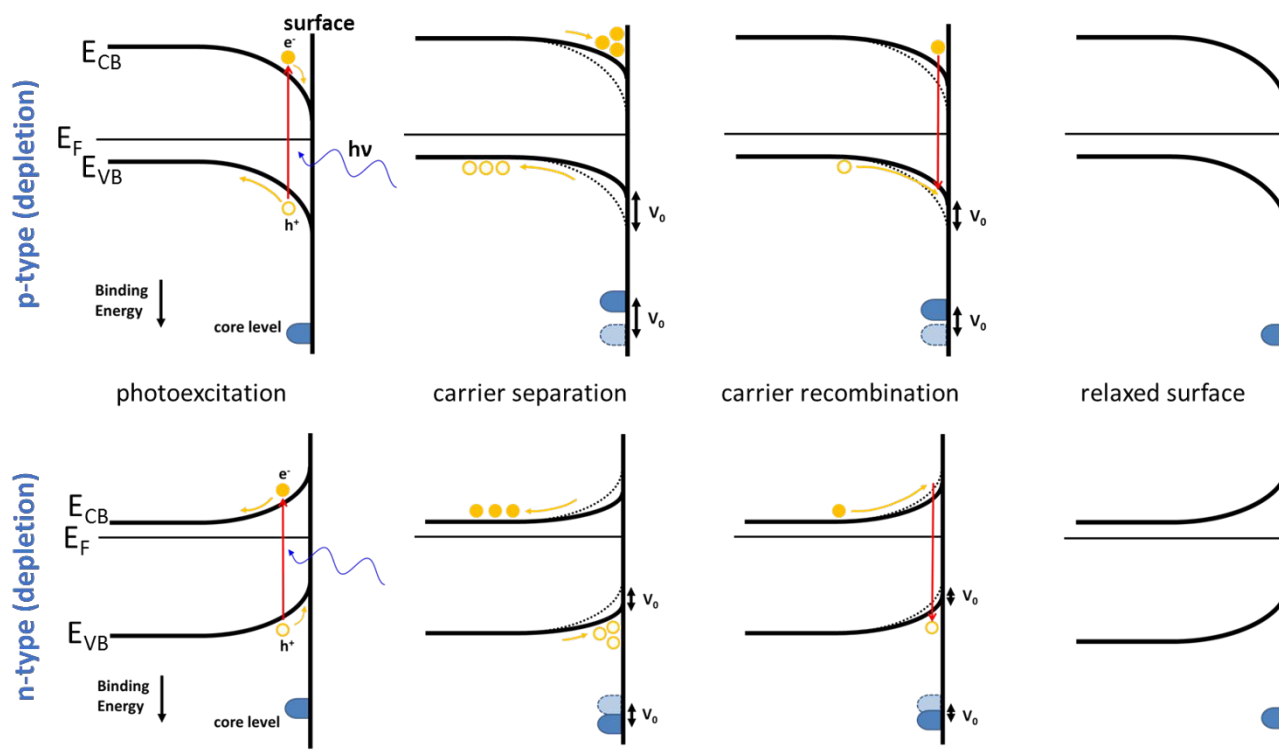
Figure 1. Schematic band diagrams of the surface photovoltage effect in (top) a p-type semiconductor material with a hole depletion layer at the surface and (bottom) an n-type semiconductor material with an electron depletion layer at the surface. The change in the band bending/size of the SPV shift (V_0) is indicated, and the position of the core levels relative to their original position is also indicated.

We present results from measurements of the SPV both in a static experiment (measuring photoemission spectra with and without a white light source incident on the CQD solid), and time-resolved measurements of the SPV shift relaxation, obtained using laser-pump photoemission-probe spectroscopy. From the former we learn that an SPV shift, due entirely to band bending rather than surface dipoles, is present at the surface of PbS CQD films. The latter technique gives additional information about the dynamics of the carriers at a semiconductor surface.[35] This method has been used to probe carrier dynamics in various semiconductor surfaces,[34,36–39] as well as to study charge injection from dyes or CQDs into transparent conducting oxides[40–43] and hole transport layers.[44] In the charge injection case, advantage is taken of the ability to probe a specific chemical species with photoemission, and therefore a specific part of the junction. Another advantage of using laser-pump photoemission-probe spectroscopy is the ability to probe the surface chemistry of a sample whilst simultaneously measuring the dynamics,[32] which we take advantage of here to aid the understanding of the time-resolved results.

Livache et al. used time-resolved SPV measurements to study HgTe nanoplatelets for use in infrared photodetector devices.[45] The technique was used to obtain the absolute lower limit for the response lifetimes of these devices (100s of ns), which was much faster than those realised (100s of μs) due to differences in carrier transport across the different geometries of the nanoplatelets. In this paper we carry out comparable measurements for CQD solids, and show that, by contrast, their intrinsic response lifetimes can be on the order of μs. This is of the same order as the lifetimes of transient photoconductivity and photovoltage dynamics reported in certain CQD-based devices.[46–49]

We also find that the surface chemistry of CQD solids has a great impact on the carrier dynamics. The presence of O_2 and H_2O contamination in the film increases the carrier lifetimes from microseconds (no contamination) to the order of seconds. This supports the idea that contaminants enable dynamic traps. Similar slow lifetimes have been observed in CQD-based field-effect transistors (FETs) by other groups.[50,51] This range of possible carrier lifetimes highlights the importance of control of the CQD solid fabrication for its intended application.

2. Experimental Section

2.1 PbS Core CQD Synthesis

PbS CQDs with different band gap energies (between 1.24 and 1.32 eV, given by the position of the first exciton peak) were synthesized by cation exchange of CdS CQDs. Details of the cation exchange procedure (using $PbCl_2$) and the synthesis of the CdS CQDs (from CdO and $(NH_4)_2S$ precursors) are given in other work.[52,53] A small amount of residual Cd was observed by

　　　　　　　　　　　　　　　　　　　　　　　　　　　　　ARTICLE

XPS in these CQDs, in amounts depending on the ligand exchange procedure used, suggesting the Cd is likely to be predominantly at the surface of the CQDs (as found in previous work).[54] Approximately ¼ of a monolayer of residual Cd is found on the surface of the PbS-MPA CQDs, and 1/12 of a monolayer on the surface of the PbS-PbI$_2$ CQDs (see supporting information Figure S1). Cd in submonolayer amounts at the surface of PbS CQDs does not significantly affect the CQD electronic structure.[55] Residual Cd was also previously observed in PbSe synthesised with the same cation exchange approach.[56] The 1.8 eV band gap CQDs were synthesized by the Hines and Scholes synthesis.[57] The ligand used during the syntheses was oleic acid (OA).

2.2 Film preparation, solid state ligand exchange and device preparation

All PbS CQD films were prepared in an inert N$_2$ environment.

PbS-EDT (1,2-ethanedithiol) films were deposited on pre-patterned ITO-coated glass. The thin PbS-EDT films were produced via dip coating using a programmable Nima Technologies Dip Coater. The substrate was first dipped into a beaker containing 5 mg ml^{-1} PbS CQDs dispersed in hexane, then slowly retracted, and dipped into a second beaker containing 2% volume EDT in acetonitrile. After slowly retracting the substrate, it was dipped into a final beaker containing pure acetonitrile. This cycle was repeated to produce one layer of CQDs. 15 layers of CQDs were deposited to produce a 45 nm-thick film.

Thicker PbS-EDT films were also prepared via spin coating. A drop of 30 mg ml^{-1} CQDs dispersed in hexane was deposited onto the spinning substrate with a spin rate of 2000 rpm, followed by two drops of 2% volume EDT in acetonitrile, and then 5 drops of pure acetonitrile. This was repeated 3 times to form one layer. 18 layers were deposited to produce a 460 nm-thick sample.

The PbS-MPA (3-mercaptopropionic acid) films were made by spin coating PbS QDs (30 mg ml^{-1} in octane) at 2000 rpm for 40 s onto a silicon substrate. The films were then immersed in a 1% v/v MPA/methanol solution for 2 seconds. This was repeated for 4 cycles to generate films approximately 100 nm thick.

PbS-PbI$_2$ films were produced with a method similar to that reported by Crisp et al. and Chernomordik et al.[6,58] PbS CQDs (30 mg ml^{-1} in octane) were deposited at 2000 rpm for 30 s onto a silicon substrate. The film was then treated by soaking in 10 mM PbI2 in DMF (dimethylformamide) for 3 minutes, then washed with acetonitrile to remove the DMF and excess PbI$_2$. This was repeated for 4 cycles to generate films approximately 100 nm thick.

PbS-MAI/PbI$_2$ (methylammonium iodide/lead iodide) CQDs were ligand exchanged in solution by methods developed by Sytnyk et al.[46] Films were made by drop-casting onto an ITO substrate and drying for 2 hours inside a glove box.

It was necessary to use CQDs synthesised by two different methods (Section 2.1) to produce the different films because the cation exchange produces films that are more stable when using ligands that are highly sensitive to air exposure (i.e. EDT and MPA).[59] This is likely to be due to the passivation from residual Cd in the CQDs (see supporting information).[55] However, in the case of PbS-MAI/PbI$_2$, the MAI/PbI$_2$ ligand exchange was found to be less reliable with cation-exchanged CQDs. Hence the Hines and Scholes synthesis method (which we observed to produce air-stable films) was used instead.

2.3 Characterization

Optical absorption spectroscopy of the CQD films was measured using a PerkinElmer Lambda 1050 UV-vis-NIR spectrophotometer. Cross-sectional scanning electron microscopy (SEM) images were taken with a Zeiss Sigma 300 electron microscope (shown in the supporting information).

XPS from core levels were recorded at room temperature in normal emission geometry, using synchrotron light linearly polarized in the horizontal plane. XPS spectra were fitted with CasaXPS.[60] The areas of the XPS peaks were corrected for photon flux and photoionization cross section.[61] Binding energies were calibrated to the literature values for PbS in S 2p.[55,62,63]

2.4 Static Photoemission Surface Photovoltage Measurements

The photoemission measurements presented in Figure 2 (Section 3.1) were performed using the BACH beamline (45 < hv < 1650 eV, equipped with a Scienta R3000 hemispherical analyzer) at the Elettra synchrotron in Trieste, Italy. Secondary electron energy distribution (SEED) measurements were measured with a sample bias of -9.5 V, and otherwise the sample was grounded. A CVLIFE SW-8066 800 lumen LED torch (focused onto the sample through a convex lens and a UV-visible window into the ultra-high vacuum (UHV) chamber) was used for static white light photoexcitation. This beamline has a glove-box-to UHV-transfer facility, so air sensitive samples were studied without exposure to air while loading.

2.5 Time-resolved Photoemission Surface Photovoltage Measurements

The laser-pump X-ray photoemission-probe time-resolved measurements presented in Section 3.2 were taken at the TEMPO beamline (50 < hv < 1500 eV, equipped with a SCIENTA SES 2002 electron energy analyzer) at Synchrotron SOLEIL, France. A continuous wave (CW) 375 nm laser (OBIS 375 nm LX 50 mW) was used for photoexcitation and modulated with a 50% duty cycle with a period adjusted to capture the dynamics of the system. Fast XPS spectra were captured at 1000 intervals over the laser cycle using a delay-line detector (with time resolution 30 ns). The sizes of the SR photoemission beam and laser photoexcitation beam at the sample position were measured with a photodiode. The SR X-ray beam was measured to have an elliptical profile with full width half maxima of 400 μm by 350 μm. The laser photoexcitation beam spot on the sample had a radius 3 times larger than the SR beam, with the latter positioned inside the laser spot allowing for uniform excitation.

ARTICLE

3. Results

3.1 Measurements using static white light illumination

First, the presence of an SPV shift in PbS-EDT CQD films was established by measuring photoemission peaks with and without photoexcitation from a white light source. The optical absorption spectrum of the PbS-EDT film used in these measurements is shown in Figure S2 in the supporting information. The 1S absorption feature is found at 1000 nm, and the film absorbs in the visible range. From the 1S peak, the effective band gap obtained is 1.24 eV, which equates to CQDs of 3.3 nm in diameter.[64] The VBM is found 0.55±0.05 eV below the E_F (from valence band photoemission in Figure S3, supporting information), indicating slight p-type behaviour.

The synchrotron radiation energy used for photoemission was hυ = 45 eV, chosen to maximise the surface sensitivity of measurements of the low binding energy (BE) core levels of the sample, so only the surface of the CQD film is probed. The SR X-ray beam was measured to have an elliptical profile of 300 μm by 100 μm. The focused white light source spot covered the whole of the CQD film. The photoemission peaks were measured repeatedly by taking spectra with the white light source switched off and on. This is necessary to check that any observed shift in the BE of the peak is due to the white light and reverses completely when the light is switched off. The Pb 5d$_{5/2}$ peak before, during, and after white light photoexcitation for a 45 nm-thick PbS-EDT CQD solid is shown in Figure 2A. This shows that there is a shift of 67 ± 3 meV to lower binding energy when the white light is on, and the peak returns to its original position after the light is turned off, so this shift is due to an effect of the light. To check whether the shift is solely due to the surface photovoltage effect (a change in band bending at the surface) or whether it could be influenced by any interface dipole present at the surface, the position of the SEED edge with and without photoexcitation was also measured, and is shown in Figure 2B. The position of the SEED edge is related to the vacuum level, so if the SEED edge shifts by the same amount as the core levels, this indicates the observed shift is entirely due to an SPV effect.[65] A shift of 68 ± 2 meV to higher kinetic energy (lower binding energy) was observed for this PbS-EDT sample confirming that the shift is due to an SPV effect. This confirms that band bending is present in these CQD films. In this case the PbS-EDT CQD film shows downward band bending at the surface that shifts towards a more flat-band situation when photoexcited carriers separate in this region. This is the behaviour anticipated at a conventional p-type semiconductor surface (Figure 1).

To investigate potential reasons for the presence of band bending at the surface of these films we measured the S 2p core level. This is a useful diagnostic of surface oxidation in PbS CQDs as there are distinct chemical shifts between different sulfur-containing oxidation products.[55,62,63,66,67] The fitted S 2p core level is shown in Figure S4, and the fitted peak BEs and assignments are shown in Table S1 in the supporting information. Spectra were measured with a photon energy of 390 eV to ensure high surface sensitivity and to enable fitting of
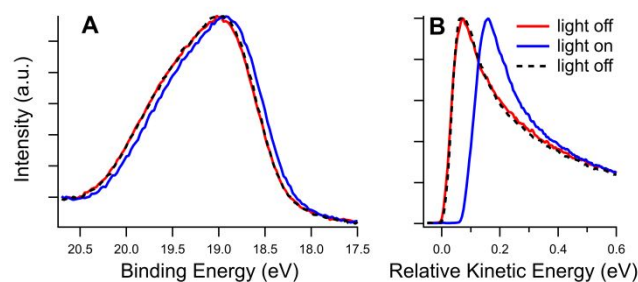

Figure 2. (A) The Pb 5d5/2 core level photoemission spectrum of a 45 nm-thick PbS-EDT CQD film. (B) Spectra of the secondary electron cutoff region. For both (A) and (B) the spectra were obtained with a photon energy of 45 eV. The spectrum is shifted to lower binding energy with white light illumination (blue). The spectra taken before (red) and after (black dashed line) white light photoexcitation show the peak returns to its original BE position after photoexcitation.

the peak without interference from the Pb 4f background that appears at higher photon energies.[55] The S 2p spectra show several oxidation products present on the surface of the PbS-EDT CQDs, including small amounts of PbSO$_3$ and PbSO$_4$ (corresponding to approximately ¼ of a monolayer, method detailed previously),[55] despite storage and sample transfer into UHV under an inert (nitrogen) environment. The presence of PbS oxidation products explains why the Pb 5d peak (Figure 2A) is broad and asymmetric. The fit to the Pb 5d spectra is shown in the Supporting Information Figure S5 and is consistent with PbSO$_3$, Pb(OH)$_2$, and PbSO$_4$ present on the surface of PbS CQDs.[55,68,69] All the fitted components were observed to shift by the same amount (67 ± 3 meV) upon photoexcitation. We consider that the nitrogen environment of the samples during travel (in a sealed CF tube) was likely to be not perfectly air free, and even small amounts of oxygen present in the environment can initiate oxidation of the PbS CQD surfaces.[70] Small amounts of oxidation in PbS-EDT CQD films (potentially occurring after desorption of ligands[71]) change the doping from n-type towards p-type.[5,19,72,73,71] Here we find the film is slightly p-type (valence band photoemission in supporting information Figure S3) with a VBM = 0.55±0.05 eV below E_F. A p-type behaviour for PbS-EDT films has also been reported by other groups.[74,75] Our VBM − E_F value is slightly lower than that measured by Brown et al. for PbS-EDT CQDs of a similar size,[5] which is consistent with the slight oxidation observed causing a more p-type behaviour in our CQD solid.

The S 2p spectrum also shows the presence of thiols from the EDT ligands in both bound and unbound states in the CQD solid. The ratio of bound to unbound thiols is 0.8±0.2:1, indicating that around half of the thiol moieties of the bidentate EDT ligands present in the films are unbound. We note that the presence of significant fully unbound EDT in the film is unlikely as it is removed by washing during spin coating but the presence of small quantities cannot be ruled out.

The same static experiment was repeated on a second PbS-EDT CQD solid of 460 nm thickness (cross sectional SEM of both films is shown in the supporting information Figure S6). Similar SPV shift results were obtained, with a shift of 62 ± 5 meV to lower binding energy in the Pb 5d$_{5/2}$ peak upon photoexcitation, and a shift of 64 ± 4 meV in the SEED edge. The surface chemistry

of this sample as determined from the S 2p core level XPS was similar to the 45 nm film (a similar ratio of bound and unbound ligands, and a small amount of sulfite and sulfate).

An interesting question is whether the oxidation products are only present on the surface of the CQD solid or are likely to be present throughout the film. CQD solids have been found to be porous to gases, and have been used to detect gases such as NO_2 and O_2 as the resistance across the CQD solid changes in the presence of the gas.[76–78] The change of the charge carrier concentrations after oxygen and water vapour exposure also suggests that PbS EDT films are porous,[72] and therefore the extent of oxidation we observe is potentially present on CQDs throughout the film, not just present on those at the surface, measured by XPS. While we cannot rule out a gradient in oxidation between CQDs in the film, it is likely that the band bending observed is not due to a difference in electronic structure of the CQDs at the surface compared to those deeper in the film. Instead it is likely to be an intrinsic feature of the CQD solid. As shown in the next section, an SPV shift demonstrating surface band bending is observed even in the absence of surface oxidation, but the extent of oxidation is important, especially in determining carrier dynamics.

3.2 Time-resolved photoemission measurements.

To probe the dynamics of the photoexcited carriers in the CQD films, time-resolved photoemission measurements were carried out at the TEMPO beamline. As no glove box transfer was available, experiments here focussed on CQD films known to be relatively air stable: PbS-MPA and PbS-PbI$_2$.[58,79,80] As our initial results indicated that the measured SPV is not dependent on film thickness, a fixed thickness of 100 nm was used. This is representative of CQD film thicknesses used in CQD-based solar cells (typically 50-400 nm).[19,23,24,81,82] The absorption spectra of both CQD solids are shown in the supporting information (Figure S2). The 1S exciton peak is found at 939 nm and 956 nm for MPA- and PbI$_2$-treated films respectively. This equates to CQDs of 3.1±0.1 nm in diameter with an effective band gap of 1.30 and 1.32 eV respectively.[64] From valence band photoemission (supporting information) the VBMs for both CQD solids were located 1.10±0.05 eV below the Fermi level, implying n-type behaviour.

For both PbS-MPA and PbS-PbI$_2$ CQD solids, fast XPS of the Pb 4f$_{7/2}$ core level, with a photon energy of hu = 475 eV was used to monitor the SPV shift at the CQD solid surface. In both cases, the dynamics were found to be dominated by slow transients, and it was necessary to use a 40 s cycle for the 'on − off' modulation of the 375 nm laser. The binding energies were extracted by fitting a sum-approximation Voigt function (with Gaussian-Lorentzian ratio 70:30) peak to the Pb 4f$_{7/2}$ level, measured over 1000 intervals during the laser cycle. An example of the SPV shift (photoexcited − unexcited) superimposed on the laser cycle profile is shown in Figure 3A.

The transient SPV shift observed for the PbS-PbI$_2$ CQD solid is shown in Figure 3B, and for the PbS-MPA CQD solid in Figure 3C. The Pb 4f core level peak shifts to higher binding energy in both cases. From the direction of the SPV shift and the knowledge

that these films are typically n-type,[83–86] we infer that there is an electron depletion layer at the surface of these CQD solids. In this case, when the laser photoexcites carriers across the band gap of CQDs at the surface of the solid, the excitons are separated by an upwards band bending at the surface. Electrons migrate away from the surface and holes travel towards it. This reduces the total band bending, creating an SPV shift. The SPV rise (onset) dynamics depend on the competition between carrier generation/separation and recombination. When the laser is turned off, the SPV shift relaxes as the excited carriers recombine (Figure 1). A simple thermionic emission model, sometimes used for fitting SPV decays of bulk semiconductors,[32,87,88] did not produce a viable fit to the data, suggesting that the dynamics are more complex, with more than one component. Instead, both the rise and decay of the SPV transients are adequately fitted with double exponentials of the form

$$SPV(t) = \Delta V \left(A_1 e^{(t-t_0)/\tau_1} + A_2 e^{(t-t_0)/\tau_2} \right) \qquad (1)$$

where ΔV is the total SPV shift, τ_1 and τ_2 are the time constants,
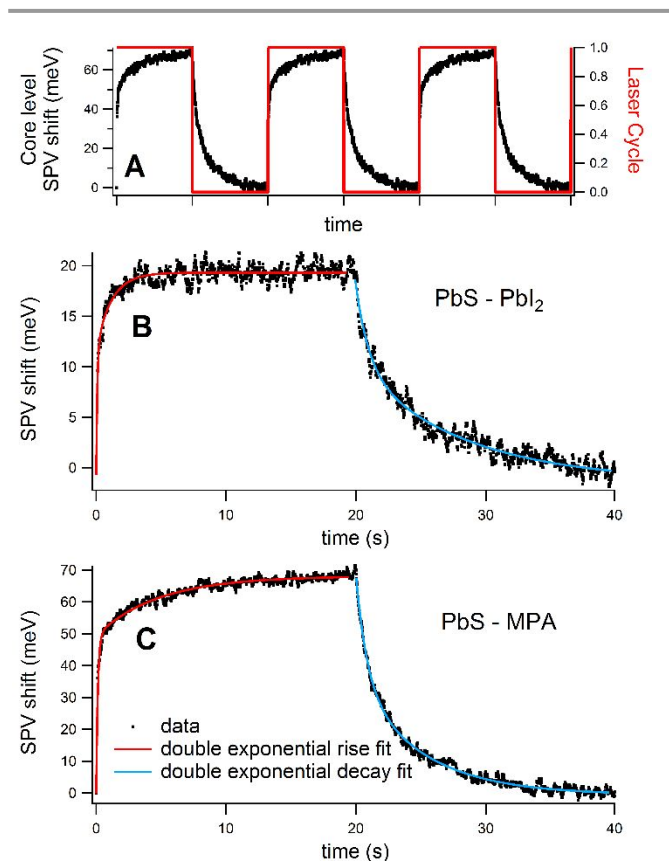

Figure 3. (A) Core level surface photovoltage (SPV) shift with the CW laser 'on-off' cycle superimposed. (B) Time-resolved SPV shift of the Pb 4f core level in a PbS CQD film treated with PbI$_2$ and (C) 3-MPA ligands under illumination by a λ = 375 nm CW laser modulated on a 50% duty cycle with a period of 40 s. The X-ray photon energy was 475 eV, corresponding to a sampling depth of 1.4 nm.[55] The rise and decay of the pump-induced SPV shift are fitted using double exponential functions (red and blue lines respectively). The fitted parameters are listed in Table **1**.

Table 1. Photoexcited carrier dynamics for samples with three different surface treatments. Note that the band gap and synthesis method were also different for the MAI/PbI$_2$ sample (see sections 2.1 and 2.2).

Ligand Treatment	SPV shift (meV)	Dynamics Time unit	Rise A1, A2	Rise τ_1	Rise τ_2	Decay A1, A2	Decay τ_1	Decay τ_2
PbI$_2$	19	s	0.47,0.53	0.1 ± 0.1	1.1 ± 0.1	0.57,0.43	1.0 ± 0.1	8.0 ± 0.5
MPA	68	s	0.42,0.58	0.1 ± 0.1	4.9 ± 0.1	0.71,0.29	0.9 ± 0.1	5.0 ± 0.1
MAI/PbI$_2$	9	μs	0.58,0.42	4.1 ± 0.5	13.5 ± 1.5	0.16,0.84	3.8 ± 1.5	13.7 ± 3.0

t_0 is a time offset (set to 0 for fitting rises, and to the 'laser off' time for fitting decays), and the constants A_1 and A_2 are constrained such that

$$A_1 + A_2 = 1. \qquad (2)$$

Similar double exponential fits have been made to transient current and voltage measurements in CQD-based FETs.[47,89,90] The total SPV shift and the rise and decay constants extracted from these fits for the PbS-PbI$_2$ and PbS-MPA CQD solids are displayed in

Table 1. In both cases the rise has two components, one faster than the other. The initial SPV rise occurs on a timescale faster than the time step in the experiment. The second rise process and both observed decay processes are slower, with time constants of the order of seconds. Reasons for these slow transients and comparisons between the extracted constants are discussed in section 4.

A third PbS-based CQD film was also studied. This was treated with MAI and PbI$_2$ to form a quasi-epitaxial metal-halide perovskite (MAPbI$_3$) ligand shell on the CQD surfaces.[46,82,91–93] The 1S absorption peak for the CQDs in this solid was at 686 nm (supporting information) giving an effective band gap of 1.81 eV and a diameter of 2.1 nm.[64] The transient SPV shift for this PbS-MAI/PbI$_2$ sample is shown in Figure 4. Immediately it is clear that the rise and decay transients in the PbS-MAI/PbI$_2$ CQD solid are observed on timescales a million times faster than those observed in the PbS-PbI$_2$ and PbS-MPA CQD solids. Reasons for this are discussed in the next section. Again these transients were also best fitted with double exponentials of the form shown in equations (1) and (2), and the fitted constants are shown in

Table 1.

The valence band photoemission (supporting information Figure S3) of the PbS-MAI/PbI$_2$ film shows that this film is close to intrinsic but slightly n-type, with a VBM = 0.95±0.05 eV below the Fermi level. The direction of the SPV shift, to higher binding energy, indicates an electron depletion region at the surface of this CQD solid. The total SPV shift observed in the PbS-MAI/PbI$_2$

sample was only 9 meV, which is smaller than the shifts observed in the PbS-PbI$_2$ and PbS-MPA films.

XPS was also used during the time-resolved measurements to quantify the species present on the surface of all the CQD solids, using the Pb 4f, S 2p, O 1s (spectra shown in supporting information Figure S4), I 3d and C 1s core levels. Each core level was measured with a different photon energy to give a resulting photoelectron kinetic energy of 335 eV. This means the photoelectrons from each core level originate from the same depth in the sample, and are probing depths of approximately 1.4 nm into the sample.[55,69,94] This was chosen to match the sampling depth of the time-resolved SPV data in Figures 3 and 4. The increased surface sensitivity attained by using low photon and photoelectron kinetic energies is one advantage of using a synchrotron radiation source for these measurements. The elemental ratios of S, I, O and C to Pb in the CQD film surfaces are displayed in Figure 5. These are discussed in context with the SPV dynamics in the next section.

4. Discussion

From the results presented here, it appears that there is intrinsic band bending at the surface of CQD solids. This suggests that electronic alignment found by UPS and other
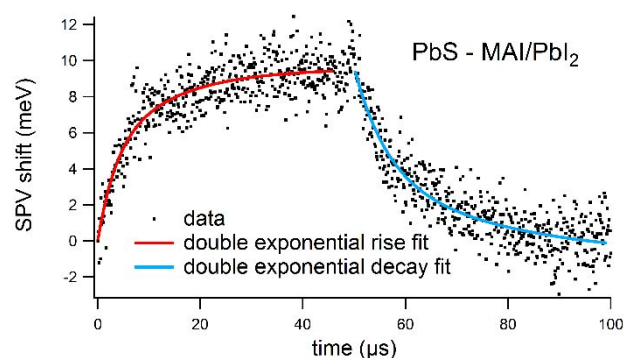

Figure 4. Time-resolved surface photovoltage (SPV) shift of the Pb 4f core level in a PbS CQD film with a quasi-epitaxial MAI/PbI$_2$ ligand shell, under illumination by a λ = 375 nm CW laser modulated on a 50% duty cycle with a period of 100 μs.
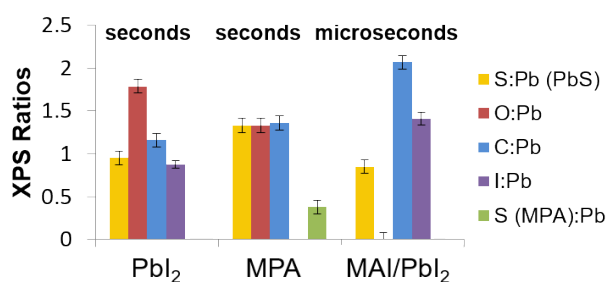
Figure 5. Ratios of elements determined from X-ray Photoelectron Spectroscopy for PbS CQDs treated with PbI$_2$, MPA, and MAI/PbI$_2$ ligands. All XPS core levels were measured at a constant sampling depth (1.4 nm) by changing the photon energy to produce photoelectrons around 335 eV in kinetic energy. The timescales for the measured SPV dynamics for each sample are shown at the top of the chart. See the supporting information for the fitted core level spectra.

surface sensitive measurements may not be representative of the bulk CQD solid, as is also the case with many conventional bulk semiconductors. However, it is still extremely important for understanding band alignment at interfaces.

In the static XPS measurements, two PbS-EDT CQD films of thicknesses 45 nm and 460 nm were studied. The size of the SPV shift under identical white light illumination was the same for both film thicknesses. This could indicate that the width of the depletion region is less than 45 nm, as the full depletion region is supported in the 45 nm thick sample; this is consistent with our observations from the time-resolved experiments as discussed below. It must be remembered however, that the thicker film was fabricated via spin coating and the thinner film via dip coating. These two methods give differences in uniformity and packing density of CQD films.[95] This affects properties such as doping carrier concentration and the absorption coefficient of the film,[72,96–98] which in turn affect the magnitude of the band bending and SPV shift upon photoexcitation.[34,99–101] Thus it may not be easy to directly compare the two PbS-EDT CQD films, due to their different fabrication processes.

For the PbS-EDT CQD solids, we observe an SPV shift to lower binding energy upon photoexcitation, and so there must be a downwards band bending at the surface of this p-type material. For both the PbS-MPA and PbS-PbI$_2$ CQD solids we observe an SPV shift to higher binding energy, and so upwards band bending at the surface of these n-type materials. On the PbS-MAI/PbI$_2$ CQD solid, we observe a small SPV shift to higher binding energy at the surface of this slightly n-type material. In all these four cases this indicates a depletion region at the surface of these CQD solids, as the surface is depleted of the majority carriers.

The formation and relaxation of an SPV shift is shown for p-type and n-type semiconductors with a space charge region at the surface in

Figure 1. For a p-type (n-type) semiconductor with a space charge region at the surface the SPV shift appears as

photoexcited electrons (holes) are driven towards the surface, while holes (electrons) migrate towards the bulk. The attraction between the electron and hole reduces the surface potential. The electrons and holes can recombine when a hole (electron) overcomes the potential barrier to the surface via thermionic emission, the rate of which is dependent on the size of the barrier. The SPV shift reaches its maximum and stays in this steady state when the carrier photoexcitation and recombination rates are equal. When returned to dark conditions, the SPV shift relaxes as carriers recombine over the surface potential. The rate of relaxation decreases as the SPV shift reduces and the potential barrier increases,[36,87] until all the photoexcited carriers have recombined and the surface is back to its dark steady-state. However, in the presence of shallow or deep trap states, the formation and relaxation times can be dominated by trapping relaxation.

Using the transient surface photovoltage shifts in Figure 3 and 4 combined with methods developed by Kronik et al. for the analysis of surface photovoltage spectroscopy, the surface band bending in the dark (V_0) was estimated for the PbS-PbI$_2$, MPA, and MAI/PbI$_2$ solids.[31,102] This involves comparing the initial gradients of the SPV transients when going between steady-state dark to light, and light to dark conditions. Details of the calculation are given in the supporting information. Schematics of the band profiles in the dark and under steady-state 375 nm laser illumination are displayed in Figure 6A-C.

The depletion width, w, at the surface of a semiconductor can be calculated knowing V_0 as

$$w = \sqrt{\frac{2\varepsilon_0\varepsilon_r V_0}{n_0 e}} \qquad (3)$$

where ε_0 and ε_r are the dielectric constant and relative permittivity respectively, n_0 is the carrier concentration, and e the electron charge.[42,103] Accurate measurement of relative permittivity and carrier concentration is difficult for these materials. They are also difficult to simulate due to a range of influencing factors including CQD size and film processing conditions.[104,105] Advances in simulating optical properties of nanostructured materials are promising; however, here we have insufficient empirical information to simulate carrier concentration and relative permittivity.[106,107] Instead, using the experimentally determined V_0 values in equation 3, the depletion widths were calculated for a range of bulk carrier concentrations[4,82,83,86,96,108] and relative permittivities[75,104,109,110] typically reported for CQD solids. The range of possible depletion widths is shown in Figure 6D-F. In some cases, low carrier concentrations produce depletion widths larger than the film thickness, which would create a more complex model where the surface depletion region would interact with the interface between the CQD solid and the substrate behind it. To simplify matters and highlight the range where the depletion region is contained within the films, the depletion width values displayed have been capped at 100 nm. Only for the lowest reported bulk carrier concentrations would the depletion widths be greater than the widths of these CQD solids. Thus, it seems reasonable that the surface
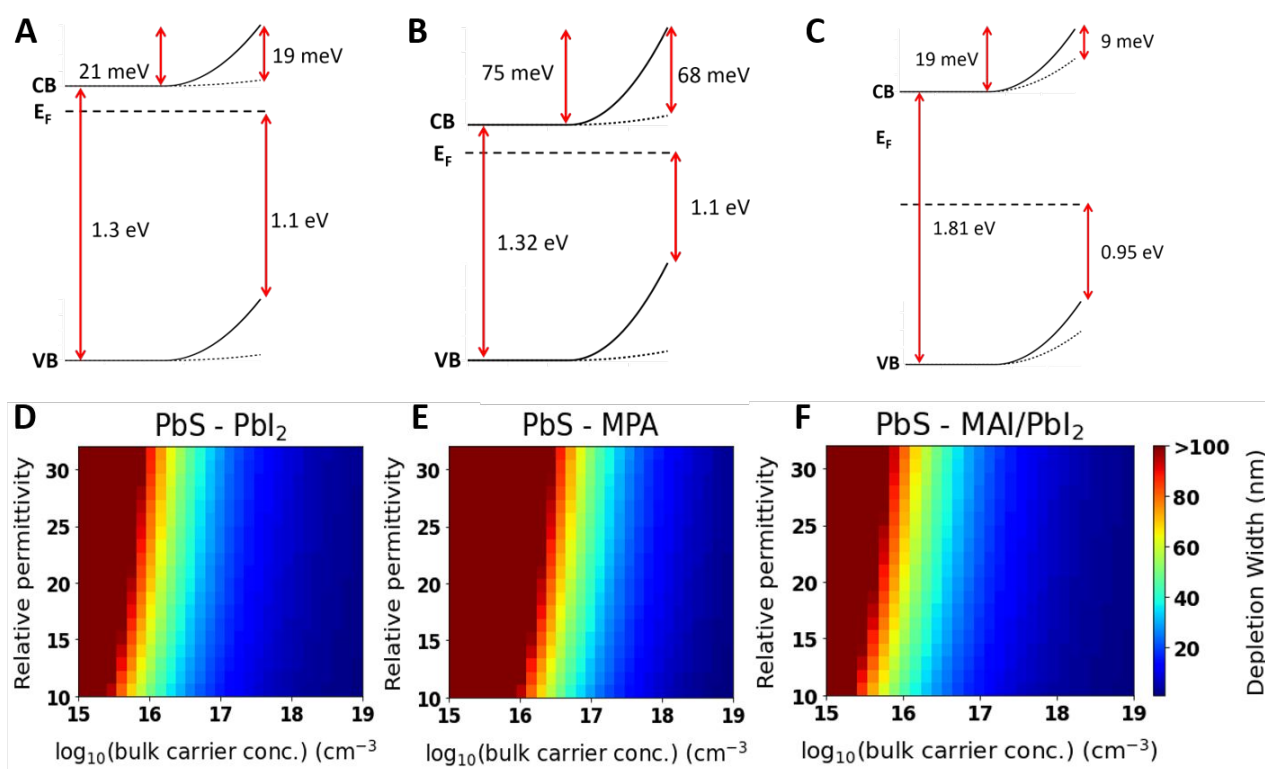
Figure 6. Schematic diagrams of the band bending at the surface of A) PbI$_2$-passivated, B) MPA-passivated and C) MAI/PbI$_2$-passivated CQD solids showing their equilibrium band bending in the dark and the maximum surface photovoltage shift observed in our experiments, as well as the band gap and Fermi level positions (not to scale). D-F) Calculated depletion widths using experimentally determined equilibrium surface band bending values over a range of relative permittivities and carrier concentrations typically reported for CQD solids.

depletion regions are typically contained within a 100 nm thick CQD film, and for the bulk concentrations expected (in the range of 7 x 10^{15} to 10^{18} cm^{-3})[4,82,83,86,96,108] the depletion region extends over some tens of nm, consistent with the indications from the static measurements. This should be taken into account in designing CQD solid devices relying upon the behaviour of the surface such as gas sensors.[76,111]

We now discuss the lifetimes observed for the different CQD solids. The second-long timescales of the transients observed for the PbS-MPA and PbS-PbI$_2$ CQD films suggests that deep traps are present in the sample, slowing down the SPV shift recovery.[45,112] These are mid-gap states arising from surface defects and other impurities. Depending on the density of the traps and their capture cross-section, they can prolong the carrier lifetime. Deep trap lifetimes in PbS-EDT CQDs have previously been estimated to be as long as 0.1 ms.[113,114] Similar timescales for transients of mobile carriers in PbS CQD-based field effect transistors (FETs) have been observed.[50,51,89,115] Zhang et al. observed exponential decays of mobile charge carrier density with time constants on the order of seconds in PbS-EDT CQD FETs.[51] They suggest that the trapping is due to reversible chemical reactions with carriers and contaminant species in the film, as they did not observe deep traps without photoexcitation. Zhang et al. suggested the dynamic trapping

mechanisms could involve hydroxyl- or hydrogen-related species, induced by the injected charge carriers, such as

$$O_2 + 2H_2O + 4e^- \rightleftharpoons 4OH^-. \tag{4}$$
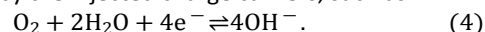
This theory is supported by the fact that they observed faster decays of mobile carriers in more humid and oxygen rich environments, as the dynamic trapping rate is increased. When the charge carriers are converted into species which are less mobile, the mobile carrier density is reduced. Although our measurements are performed in UHV, there is evidence for O$_2$ and H$_2$O species being incorporated into CQD films after fabrication and ligand exchange.[67,72,116–119]

The presence of oxygen-containing species on the surface of our PbS-MPA and PbS-PbI$_2$ CQD films was confirmed by O 1s XPS (supporting information and Figure 5). The formation of dynamic deep traps activated by photoexcited carriers is consistent with the timescales of the rise and decay we observe in these films. In our case we observe a greater SPV shift when more carriers are separated across a depletion region at the surface, and the shift decreases as the carriers recombine. During the rise ('laser on' period), photoexcitation and recombination are competing. When photoexcited carriers are separated over the depletion region, if for example an electron reacts with O$_2$ and/or H$_2$O to form OH$^-$, the OH$^-$ is less mobile than the electron and is not able to migrate back to the surface to recombine with a hole until the OH$^-$ reverts to an electron

which is mobile enough to migrate. If excess O_2/H_2O is available then more electrons can be trapped and the electron-hole recombination rate is reduced, reducing the rise time. During the decay ('laser off' period), only the recombination of carriers contributes to reduction in SPV shift. The carriers must be mobile (not in traps) to spatially overlap and recombine. While a carrier is trapped outside of the depletion region as a less-mobile species its contribution to the SPV shift remains. Essentially, if the dynamic trapping rate is increased then the recombination rate is reduced, and the SPV shift decay times increase.

Both the rise and decays in the time-resolved results for PbS-MPA and PbS-PbI$_2$ (Figure 3) were best fitted with double exponential equations of the form of equation (1) with the constraint expressed in equation (2). Double exponential fits have been used previously for photovoltage decays in CQD-based and perovskite-based solar cell devices.[47,89,90,120] Thus there are two processes contributing to the SPV shift generation and relaxation in each case. Discussing first the onset (rise) of the SPV shift, the initial process occurs on timescales faster than 0.1 s (the time-step size for these measurements). This suggests electrons and holes are initially able to migrate to the bulk and surface respectively without being trapped with a lifetime shorter than 0.1 s (which is over an order of magnitude faster than the trapping lifetimes observed by Zhang et al.[51]). The second process is slower, and slower in the PbS-MPA film than in PbS-PbI$_2$. As shown in Figure 5, the PbS-PbI$_2$ film has a higher ratio of O:Pb than PbS-MPA.   Comparing the O 1s spectra of these two samples (supporting information) we find a larger feature in the region that can be attributed to species such as O_2 and H_2O in the surface of the PbS-PbI$_2$ film compared to the PbS-MPA film.[67,96,121–123] This agrees with the idea that having more O_2 and H_2O available to react with excited carriers to form dynamic traps results in a shorter rise lifetime (rise τ_2 in Table 2).

Turning now to the decay of the SPV shift, the two decay lifetimes appear due to two different dynamic trap formation mechanisms. The τ_1 decay is the same for the two films, so results from a process that is equally likely in both. Considering the τ_2 decay lifetime, we find this is longer in the PbS-PbI$_2$ film than in the PbS-MPA film, as would be expected if more dynamic traps can be formed as described above.

It is unlikely that the difference in the ligands contribute to the difference in the slow τ_2 lifetimes observed. Time constants associated with shallow trap states due to unpassivated surface sites states typically have faster lifetimes, on ps to µs scales.[120,124–128] Changes due to differences in CQD spacing in the solid are also not probable since transients associated with inter-CQD transfer also occur on much shorter timescales.[129–131] The other CQD film that was studied with time-resolved photoemission received a MAI and PbI$_2$ treatment to form a quasi-epitaxial metal-halide perovskite ligand shell on the CQD surfaces. CQD solids produced with this technique have previously been shown to be nearly defect free.[46] From the ratios presented in Figure 5 we see that the amount of oxygen present in this PbS-MAI/PbI$_2$ film is below the detection limits of XPS, while the PbS-MPA and PbI$_2$ films have a considerable

amount (see O 1s spectra in the supporting information). The SPV dynamics recorded for the PbS-MAI/PbI$_2$ film, presented in Table **1** and Figure 4 are also on the order of 10^6 times faster than those in the films with higher oxygen contents. These timescales are much more consistent with those observed in bulk semiconductors such as Si, dominated by carrier recombination across the band gap.[32] This suggests that upon photoexcitation dynamic traps are not able to form in these films because the O_2/H_2O required to form them are not available. Instead, faster mechanisms dominate.

Recently Sytnyk et al. reported transient photoconductivity for a PbS CQD solid treated with MAI and BiI$_6$ ligands, fitted with an exponential decay that yields a lifetime (69 µs) of the same order of magnitude as the lifetimes we observe here for the PbS-MAI/PbI$_2$ CQD solid. Zhang et al. also reported similar transient lifetimes in solar cells based on CsPbI$_3$ coated PbS CQDs.[49]

The difference in oxygenation is not the only difference between the PbS-MAI/PbI$_2$ CQD solid and the PbS-MPA and PbI$_2$ films. Although it was necessary to use a different synthesis procedure to produce the PbS CQDs making up the PbS-MAI/PbI$_2$ film, there are no significant differences in electronic structure (see section 2.1 and supplementary information Figure S3).[55] Other differences include the size of the CQDs (2.1 nm vs 3.1 nm respectively), and the different ligands resulting in different interdot distances and packing densities.[4,48,63,92,132–134] Although these are likely to have some effect on the SPV dynamics, we believe a key factor in the 6 orders of magnitude difference in lifetimes is the difference in the levels of O-containing contamination, with the latter resulting in trap states which increase the lifetimes of photoexcited carriers.

The time-resolved laser-pump X-ray photoemission-probe results suggest that the surface chemistry of the CQD solids dominates the timescales of the carrier dynamics. Where dynamic deep trap formation is possible, the dominant dynamics occur on a second timescale; when it is not, they occur on a microsecond timescale. Both timescales are desirable for different optoelectronic applications. For example, longer lifetimes of photoexcited carriers are preferable in photovoltaic devices,[135,136] photoconductors,[137] imaging,[138] and memory devices,[139] as there is more opportunity for carrier extraction, provided the carriers can be detrapped. On the other hand, faster excitation and relaxation dynamics are preferred in devices which require fast on/off responses such as field effect transistors or photodetectors.

Finally, we note that we have observed surface band bending in CQD films made by a number of preparatory routes with a number of ligands, in the presence and absence of differing amounts of oxygenation. This suggests that surface band bending should be universally observable in other semiconductor material CQD systems, although the degree of band bending will be dependent on the material, CQD properties, the density of carriers and/or defects and film processing conditions. We would also expect films made from ordered nano-objects of different dimensionalities to also exhibit surface band bending along the confined dimension(s), and indeed, film-scale band bending has been observed in

nanoplatelet colloidal quantum well films.[45] Dimensionality, shape, size, spacing, and the ligands of the nano-objects used in nanomaterial films should also affect the surface band bending features just as they effect optical and electronic properties.[140–142]

5. Conclusions

By using photoemission techniques to measure a surface photovoltage shift upon photoexcitation with visible light sources we have shown that band bending is intrinsic to CQD solids and occurs at the CQD solid-vacuum interface. It is observed in the presence and in the absence of detectable surface oxygenation, and for a number of ligand types and synthesis routes. We observed space charge regions at the surface of p-type and n-type CQD solids. This has implications for energy band alignments inferred from surface sensitive techniques, which may not be representative of the bulk of the film.

Time-resolved laser-pump X-ray photoemission-probe measurements were used to measure the photoexcited carrier dynamics at the surface of CQD films. We extracted depletion layer widths that are likely to be accommodated within 100 nm thick films which suggest that the timescale of the photoexcited SPV dynamics depends on the surface chemistry of the film. If large amounts of oxygen-containing contaminants are present in the film, the SPV shift lifetimes increase by 6 orders of magnitudes compared to a film with no observable contamination. This is consistent with the idea of dynamic deep trap formation, when photoexcited carriers react with contaminants, decreasing the mobility of the photoexcited carriers.[51,143] Further work is needed to study the interplay between the surface band bending and the degree of oxidation. Our work highlights the importance of characterising and understanding contaminants in CQD solids as well as degradation and passivation. By using the surface chemistry to control the photoexcited carrier lifetimes, CQD solids can be tailored to different applications. The advantage of using a time-resolved photoemission technique to study the dynamics is that the surface chemistry can be measured simultaneously. More measurements of this kind would be useful to determine the influence of other factors such as ligand passivation, CQD size and packing density on the SPV dynamics.

Conflicts of interest

There are no conflicts to declare.

Acknowledgements

Notes and references

1   H. Goodwin, T. C. Jellicoe, N. J. L. K. Davis and M. L. Böhm, *Nanophotonics*, 2018, **7**, 111–126.

2   M. C. Beard, J. M. Luther, O. E. Semonin and A. J. Nozik, *Acc. Chem. Res.*, 2012, **46**, 1252–1260.

3   S. Koley, J. Cui, Y. E. Panfil and U. Banin, *Acc. Chem. Res.*, 2021, **54**, 1178–1188.

4   C. R. Kagan and C. B. Murray, *Nat. Nanotechnol.*, 2015, **10**, 1013–1026.

5   P. R. Brown, D. Kim, R. R. Lunt, N. Zhao, M. G. Bawendi, J. C. Grossman and V. Bulovi, *ACS Nano*, 2014, **8**, 5863–5872.

6   R. W. Crisp, D. M. Kroupa, A. R. Marshall, E. M. Miller, J. Zhang, M. C. Beard and J. M. Luther, *Sci. Rep.*, 2015, **5**, 9945.

7   S. J. Oh, N. E. Berry, J. H. Choi, E. A. Gaulding, H. Lin, T. Paik, B. T. Diroll, S. Muramoto, C. B. Murray and C. R. Kagan, *Nano Lett.*, 2014, **14**, 1559–1566.

8   M. A. Boles, D. Ling, T. Hyeon and D. V. Talapin, *Nat. Mater.*, 2016, **15**, 141–153.

9   W. Chen, J. Zhong, J. Li, N. Saxena, L. P. Kreuzer, H. Liu, L. Song, B. Su, D. Yang, K. Wang, J. Schlipf, V. Körstgens, T. He, K. Wang and P. Müller-Buschbaum, *J. Phys. Chem. Lett.*, 2019, **10**, 2058–2065.

10   R. Miranti, D. Shin, R. D. Septianto, M. Ibáñez, M. V. Kovalenko, N. Matsushita, Y. Iwasa and S. Z. Bisri, *ACS Nano*, 2020, **14**, 3242–3250.

11   E. M. Sanehira, A. R. Marshall, J. A. Christians, S. P. Harvey, P. N. Ciesielski, L. M. Wheeler, P. Schulz, L. Y. Lin, M. C. Beard and J. M. Luther, *Sci. Adv.*, 2017, **3**, eaao4204.

12   M. Hao, Y. Bai, S. Zeiske, L. Ren, J. Liu, Y. Yuan, N. Zarrabi, N. Cheng, M. Ghasemi, P. Chen, M. Lyu, D. He, J. H. Yun, Y. Du, Y. Wang, S. Ding, A. Armin, P. Meredith, G. Liu, H. M. Cheng and L. Wang, *Nat. Energy*, 2020, **5**, 79–88.

13   K. T. Shimizu, M. Böhmer, D. Estrada, S. Gangwal, S. Grabowski, H. Bechtel, E. Kang, K. J. Vampola, D. Chamberlin, O. B. Shchekin and J. Bhardwaj, *Photonics Res.*, 2017, **5**, A1–A6.

14   F. Fan, O. Voznyy, R. P. Sabatini, K. T. Bicanic, M. M. Adachi, J. R. McBride, K. R. Reid, Y. S. Park, X. Li, A. Jain, R. Quintero-Bermudez, M. Saravanapavanantham, M. Liu, M. Korkusinski, P. Hawrylak, V. I. Klimov, S. J. Rosenthal, S. Hoogland and E. H. Sargent, *Nature*, 2017, **544**, 75–79.

15   A. Maulu, P. J. Rodríguez Cantó, J. Navarro Arenas, R. Abargues, J. F. Sanchez-Royo, R. García Calzada and J. P. Martínez-Pastor, *RSC Adv.*, 2016, **6**, 80201–80212.

16   A. Yousefiamin, N. A. Killilea, M. Sytnyk, P. Maisch, K. C.

Tam, H. J. Egelhaaf, S. Langner, T. Stubhan, C. J. Brabec, T. Rejek, M. Halik, K. Poulsen, J. Niehaus, A. Köck and W. Heiss, *ACS Nano*, 2019, **13**, 2389–2397.

17   I. Ramiro, O. Özdemir, S. Christodoulou, S. Gupta, M. Dalmases, I. Torre and G. Konstantatos, *Nano Lett.*, 2020, **20**, 1003–1008.

18   N. Oh, B. H. Kim, S. Cho, S. Nam, S. P. Rogers, Y. Yu, Y. K. Cho, G. Hur, J. Zhang and P. Trefonas, *Science*, 2017, **355**, 616–619.

19   C.-H. M. Chuang, P. R. Brown, V. Bulović and M. G. Bawendi, 2014, **13**, 796–801.

20   A. G. Pattantyus-abraham, Ќ. I. J. Kramer, Ќ. A. R. Barkhouse, X. Wang, G. Konstantatos, R. Debnath, L. Levina, I. Raabe, M. K. Nazeeruddin and E. H. Sargent, *ACS Nano*, 2010, **4**, 3374–3380.

21   H. Hosokawa, R. Tamaki, T. Sawada, A. Okonogi, H. Sato, Y. Ogomi, S. Hayase, Y. Okada and T. Yano, *Nat. Commun.*, 2019, **10**, 4–6.

22   G. Shi, Y. Wang, Z. Liu, L. Han, J. Liu, Y. Wang, K. Lu, S. Chen, X. Ling, Y. Li, S. Cheng and W. Ma, *Adv. Energy Mater.*, 2017, **7**, 1602667.

23   R. Azmi, S. Sinaga, H. Aqoma, G. Seo, T. Kyu and M. Park, *Nano Energy*, 2017, **39**, 86–94.

24   X. Yao, Z. Song, L. Mi, G. Li, X. Wang, X. Wang and Y. Jiang, *Sol. Energy Mater. Sol. Cells*, 2017, **164**, 122–127.

25   E. Kalesaki, W. H. Evers, G. Allan, D. Vanmaekelbergh and C. Delerue, *Phys. Rev. B*, 2013, **88**, 115431.

26   M. C. Weidman, D. M. Smilgies and W. A. Tisdale, *Nat. Mater.*, 2016, **15**, 775–781.

27   J. H. Choi, A. T. Fafarman, S. J. Oh, D. K. Ko, D. K. Kim, B. T. Diroll, S. Muramoto, J. G. Gillen, C. B. Murray and C. R. Kagan, *Nano Lett.*, 2012, **12**, 2631–2638.

28   T. G. Kim, H. Choi, S. Jeong and J. W. Kim, *J. Phys. Chem. C*, 2014, **118**, 27884–27889.

29   D. C. J. Neo, S. D. Stranks, G. E. Eperon, H. J. Snaith, H. E. Assender and A. R. Andrew, *Appl. Phys. Lett.*, 2015, **107**, 103902.

30   M. Liu, F. P. G. de Arquer, Y. Li, X. Lan, G. H. Kim, O. Voznyy, L. K. Jagadamma, A. S. Abbas, S. Hoogland, Z. Lu, J. Y. Kim, A. Amassian and E. H. Sargent, *Adv. Mater.*, 2016, **28**, 4142–4148.

31   L. Kronik and Y. Shapira, *Surf. Sci. Rep.*, 1999, **37**, 1–206.

32   B. F. Spencer, D. M. Graham, S. J. O. Hardman, E. A. Seddon, M. J. Cliffe, K. L. Syres, A. G. Thomas, S. K. Stubbs, F. Sirotti, M. G. Silly, P. F. Kirkham, A. R. Kumarasinghe, G. J. Hirst, A. J. Moss, S. F. Hill, D. A. Shaw, S. Chattopadhyay and W. R. Flavell, *Phys. Rev. B*, 2013, **88**, 195301.

33   B. F. Spencer, M. J. Cliffe, D. M. Graham, S. J. O. Hardman, E. a Seddon, K. L. Syres, A. G. Thomas, F. Sirotti, M. G. Silly, J. Akhtar, P. O'Brien, S. M. Fairclough, J. M. Smith, S. Chattopadhyay and W. R. Flavell, *Faraday Discuss.*, 2014, **171**, 275–98.

34   S. Tanaka, S. D. Moré, K. Takahashi and M. Kamada, *J. Phys. Soc. Japan*, 2003, **72**, 659–663.

35   T. Gießel, D. Bröcker, P. Schmidt and W. Widdra, *Rev. Sci. Instrum.*, 2003, **74**, 4620.

36   W. Widdra, D. Bröcker, T. Gießel, I. V Hertel, W. Krüger, A.

Liero, F. Noack, V. Petrov, D. Pop, P. M. Schmidt, R. Weber, I. Will and B. Winter, *Surf. Sci.*, 2003, **543**, 87–94.

37   K. Ozawa, M. Emori, S. Yamamoto, R. Yukawa, S. Yamamoto, R. Hobara, K. Fujikawa, H. Sakama and I. Matsuda, *J. Phys. Chem. Lett*, 2014, **5**, 1953–1957.

38   R. Yukawa, S. Yamamoto, K. Ozawa, M. Emori, M. Ogawa, S. Yamamoto, K. Fujikawa, R. Hobara, S. Kitagawa, H. Daimon, H. Sakama and I. Matsuda, *Appl. Phys. Lett.*, 2014, **105**, 151602.

39   D. Amelot, P. Rastogi, B. Martinez, C. Gréboval, C. Livache, F. A. Bresciani, J. Qu, A. Chu, M. Goyal, S.-S. Chee, N. Casaretto, X. Z. Xu, C. Méthivier, H. Cruguel, A. Ouerghi, A. Nag, M. G. Silly, N. Witkowski and E. Lhuillier, *J. Phys. Chem. C*, 2020, **124**, 3873–3880.

40   S. Neppl, A. Shavorskiy, I. Zegkinoglou, M. Fraund, D. S. Slaughter, T. Troy, M. P. Ziemkiewicz, M. Ahmed, S. Gul, B. Rude, J. Z. Zhang, A. S. Tremsin, P.-A. Glans, Y.-S. Liu, C. H. Wu, J. Guo, M. Salmeron, H. Bluhm and O. Gessner, *Faraday Discuss.*, 2014, **171**, 219.

41   A. Shavorskiy, A. Cordones, J. Vura-Weis, K. Siefermann, D. Slaughter, F. Sturm, F. Weise, H. Bluhm, M. Strader, H. Cho, M.-F. Lin, C. Bacellar, C. Khurmi, M. Hertlein, J. Guo, T. Tyliszczak, D. Prendergast, G. Coslovich, J. Robinson, R. a. Kaindl, R. W. Schoenlein, A. Belkacem, T. Weber, D. M. Neumark, S. R. Leone, D. Nordlund, H. Ogasawara, A. R. Nilsson, O. Krupin, J. J. Turner, W. F. Schlotter, M. R. Holmes, P. a. Heimann, M. Messerschmidt, M. P. Minitti, M. Beye, S. Gul, J. Z. Zhang, N. Huse and O. Gessner, 2013, **475**, 475–479.

42   B. F. Spencer, M. A. Leontiadou, P. C. J. Clark, A. Williamson, M. G. Silly, F. Sirotti, S. M. Fairclough, D. C. J. Neo, A. A. R. Watt and W. R. Flavell, *Appl. Phys. Lett.*, 2016, **108**, 091603.

43   T. Sloboda, S. Svanström, F. O. L. Johansson, A. Andruszkiewicz, X. Zhang, E. Giangrisostomi, R. Ovsyannikov, A. Föhlisch, S. Svensson, N. Mårtensson, E. M. J. Johansson, A. Lindblad, H. Rensmo and U. B. Cappel, *Sci. Rep.*, 2020, **10**, 22438.

44   C. Gréboval, P. Rastogi, J. Qu, A. Chu, J. Ramade, A. Khalili, C. Dabard, T. H. Dang, H. Cruguel, A. Ouerghi, N. Witkowski, M. G. Silly and E. Lhuillier, *J. Phys. Chem. C*, 2020, **124**, 23400–23409.

45   C. Livache, E. Izquierdo, B. Martinez, M. Dufour, D. Pierucci, S. Keuleyan, H. Cruguel, L. Becerra, J. L. Fave, H. Aubin, A. Ouerghi, E. Lacaze, M. G. Silly, B. Dubertret, S. Ithurria and E. Lhuillier, *Nano Lett.*, 2017, **17**, 4067–4074.

46   M. Sytnyk, S. Yakunin, W. Schöfberger, R. T. Lechner, M. Burian, L. Ludescher, N. A. Killilea, A. Yousefiamin, D. Kriegner, J. Stangl, H. Groiss and W. Heiss, *ACS Nano*, 2017, **11**, 1246–1256.

47   V. Malgras, G. Zhang, A. Nattestad, T. M. Clarke, A. J. Mozer, Y. Yamauchi and J. H. Kim, *ACS Appl. Mater. Interfaces*, 2015, **7**, 26455–26460.

48   K. S. Jeong, J. Tang, H. Liu, J. Kim, A. W. Schaefer, K. Kemp, L. Levina, X. Wang, S. Hoogland, R. Debnath, L. Brzozowski, E. H. Sargent and J. B. Asbury, *ACS Nano*, 2012, **6**, 89–99.

49   X. Zhang, J. Zhang, D. Phuyal, J. Du, L. Tian, V. A. Öberg, M.

B. Johansson, U. B. Cappel, O. Karis, J. Liu, H. Rensmo, G. Boschloo and E. M. J. Johansson, *Adv. Energy Mater.*, 2018, **8**, 1702049.

50   T. P. Osedach, N. Zhao, T. L. Andrew, P. R. Brown, D. D. Wanger, D. B. Strasfeld, L. Y. Chang, M. G. Bawendi and V. Bulovic, *ACS Nano*, 2012, **6**, 3121–3127.

51   Y. Zhang, Q. Chen, A. P. Alivisatos and M. Salmeron, *Nano Lett.*, 2015, **15**, 4647–4663.

52   J. Zhang, B. D. Chernomordik, R. W. Crisp, D. M. Kroupa, J. M. Luther, E. M. Miller, J. Gao and M. C. Beard, *ACS Nano*, 2015, **9**, 7151–7163.

53   Y. Yan, R. W. Crisp, J. Gu, B. D. Chernomordik, G. F. Pach, A. R. Marshall, J. A. Turner and M. C. Beard, *Nat. Energy*, 2017, **2**, 17052.

54   P. C. J. Clark, D. C. J. Neo, R. Ahumada-Lazo, A. I. Williamson, I. Pis, S. Nappini, A. A. R. Watt and W. R. Flavell, *Langmuir*, 2018, **34**, 8887–8897.

55   P. C. J. Clark, H. Radtke, A. Pengpad, A. I. Williamson, B. F. Spencer, J. O. Hardman, M. A. Leontiadou, D. C. J. Neo, S. M. Fairclough, A. A. R. Watt, I. Pis, S. Nappini, F. Bondino, E. Magnano, K. Schulte, M. Silly, F. Sirotti and W. R. Flavell, *Nanoscale*, 2017, **9**, 6056–6067.

56   J. Zhang, J. Gao, C. P. Church, E. M. Miller, J. M. Luther, V. I. Klimov and M. C. Beard, *Nano Lett.*, 2014, **14**, 6010–6015.

57   M. A. Hines and G. D. Scholes, *Adv. Mater.*, 2003, **15**, 1844–1849.

58   B. D. Chernomordik, A. R. Marshall, G. F. Pach, J. M. Luther and M. C. Beard, *Chem. Mater.*, 2017, **29**, 189–198.

59   W. Gao, G. Zhai, C. Zhang, Z. Shao, L. Zheng, Y. Zhang, Y. Yang, X. Li, X. Liu and B. Xu, *RSC Adv.*, 2018, **8**, 15149–15157.

60   *CasaXPS version 2.3.16*, Casa Software Ltd, 2011.

61   J. J. Yeh, *Atomic Calculation of Photoionization Cross-Sections and Asymmetry Parameters*, Gordon and Breach Science Publishers, Langhorne, PE, 1993.

62   G. Wittstock, I. Kartio, D. Hirsch, S. Kunze and R. Szargan, *Langmuir*, 1996, **12**, 5709–5721.

63   A. H. Ip, S. M. Thon, S. Hoogland, O. Voznyy, D. Zhitomirsky, R. Debnath, L. Levina, L. R. Rollny, G. H. Carey, A. Fischer, K. W. Kemp, I. J. Kramer, Z. Ning, A. J. Labelle, K. W. Chou, A. Amassian and E. H. Sargent, *Nat. Nanotechnol.*, 2012, **7**, 577–582.

64   I. Moreels, K. Lambert, D. Smeets, D. De Muynck, T. Nollet, J. C. Martins, F. Vanhaecke, A. Vantomme, C. Delerue, G. Allan and Z. Hens, *ACS Nano*, 2009, **3**, 3023–3030.

65   D. C. Gleason-Rohrer, B. S. Brunschwig and N. S. Lewis, *J. Phys. Chem. C*, 2013, **117**, 18031–18042.

66   A. Lobo, T. Möller, M. Nagel, H. Borchert, S. G. Hickey and H. Weller, *J. Phys. Chem. B*, 2005, **109**, 17422–17428.

67   Y. Cao, A. Stavrinadis, T. Lasanta, D. So and G. Konstantatos, *Nat. Energy*, 2016, **1**, 16035.

68   L. V. Yashina, A. S. Zyubin, R. Püttner, T. S. Zyubina, V. S. Neudachina, P. Stojanov, J. Riley, S. N. Dedyulin, M. M. Brzhezinskaya and V. I. Shtanov, *Surf. Sci.*, 2011, **605**, 473–482.

69   D. J. H. Cant, K. L. Syres, P. J. B. Lunt, H. Radtke, J. Treacy, P. J. Thomas, E. A. Lewis, S. J. Haigh, P. O. Brien, K. Schulte, F.

Bondino, E. Magnano and W. R. Flavell, *Langmuir*, 2015, **31**, 1445–1453.

70   S. J. O. Hardman, D. M. Graham, S. K. Stubbs, B. F. Spencer, E. A. Seddon, H.-T. Fung, S. Gardonio, F. Sirotti, M. G. Silly, J. Akhtar, P. O'Brien, D. J. Binks and W. R. Flavell, *Phys. Chem. Chem. Phys.*, 2011, **13**, 20275–20283.

71   M. H. Zarghami, Y. Liu, M. Gibbs, E. Gebremichael, C. Webster and M. Law, *ACS Nano*, 2010, **4**, 2475–2485.

72   D. M. Balazs, M. I. Nugraha, S. Z. Bisri, M. Sytnyk, W. Heiss and M. a. Loi, *Appl. Phys. Lett.*, 2014, **104**, 112104.

73   A. R. Kirmani, A. D. Sheikh, M. R. Niazi, M. A. Haque, M. Liu, F. P. G. de Arquer, J. Xu, B. Sun, O. Voznyy, N. Gasparini, D. Baran, T. Wu, E. H. Sargent and A. Amassian, *Adv. Mater.*, 2018, 1801661.

74   C.-H. M. Chuang, P. R. Brown, V. Bulović and M. G. Bawendi, *Nat. Mater.*, 2014, **13**, 796–801.

75   L. Hu, Z. Zhang, R. J. Patterson, Y. Hu, W. Chen, C. Chen, D. Li, C. Hu, C. Ge, Z. Chen, L. Yuan, C. Yan, N. Song, Z. L. Teh, G. J. Conibeer, J. Tang and S. Huang, *Nano Energy*, 2018, **46**, 212–219.

76   H. Liu, M. Li, O. Voznyy, L. Hu, Q. Fu, D. Zhou, Z. Xia, E. H. Sargent and J. Tang, *Adv. Mater.*, 2014, **26**, 2718–2724.

77   V. V. Burungale, R. S. Devan, S. A. Pawar, N. S. Harale, V. L. Patil, V. K. Rao, Y. R. Ma, J. E. Ae, J. H. Kim and P. S. Patil, *Mater. Sci. Pol.*, 2016, **34**, 204–211.

78   L. Maserati, I. Moreels, M. Prato, R. Krahne, L. Manna and Y. Zhang, *ACS Appl. Mater. Interfaces*, 2014, **6**, 9517–9523.

79   S. Kim, A. R. Marshall, D. M. Kroupa, E. M. Miller, J. M. Luther, S. Jeong and M. C. Beard, *ACS Nano*, 2015, **9**, 8157–8164.

80   Z. Ning, O. Voznyy, J. Pan, S. Hoogland, V. Adinolfi, J. Xu, M. Li, A. R. Kirmani, J.-P. Sun, J. Minor, K. W. Kemp, H. Dong, L. Rollny, A. Labelle, G. Carey, B. Sutherland, I. Hill, A. Amassian, H. Liu, J. Tang, O. M. Bakr and E. H. Sargent, *Nat. Mater.*, 2014, **13**, 822–828.

81   A. R. Kirmani, G. H. Carey, M. Abdelsamie, B. Yan, D. Cha, L. R. Rollny, X. Cui, E. H. Sargent and A. Amassian, *Adv. Mater.*, 2014, **26**, 4717–4723.

82   Z. Yang, A. Janmohamed, X. Lan, F. P. García De Arquer, O. Voznyy, E. Yassitepe, G. H. Kim, Z. Ning, X. Gong, R. Comin and E. H. Sargent, *Nano Lett.*, 2015, **15**, 7539–7543.

83   A. R. Kirmani, A. Kiani, M. M. Said, O. Voznyy, N. Wehbe, G. Walters, S. Barlow, E. H. Sargent, S. R. Marder and A. Amassian, *ACS Energy Lett.*, 2016, **1**, 922–930.

84   O. Voznyy, D. Zhitomirsky, P. Stadler, Z. Ning, S. Hoogland and E. H. Sargent, *ACS Nano*, 2012, **6**, 8448–8455.

85   Z. L. Teh, L. Hu, Z. Zhang, A. R. Gentle, Z. Chen, Y. Gao, L. Yuan, Y. Hu, T. Wu, R. J. Patterson and S. Huang, *ACS Appl. Mater. Interfaces*, 2020, **12**, 22751–22759.

86   M. I. Nugraha, S. Kumagai, S. Watanabe, M. Sytnyk, W. Heiss, M. A. Loi and J. Takeya, *ACS Appl. Mater. Interfaces*, 2017, **9**, 18039–18045.

87   D. Bröcker, T. Gießel and W. Widdra, *Chem. Phys.*, 2004, **299**, 247–251.

88   M. Ogawa, S. Yamamoto, R. Yukawa, R. Hobara, C. H. Lin, R. Y. Liu, S. J. Tang and I. Matsuda, *Phys. Rev. B*, 2013, **87**, 2–5.

89   Y. Kim, H. Ko and B. Park, *J. Phys. D Appl. Phys.*, 2018, **51**,

145306.

90   B. C. O'Regan, P. R. F. Barnes, X. Li, C. Law, E. Palomares and J. M. Marin-Beloqui, *J. Am. Chem. Soc.*, 2015, **137**, 5087–5099.

91   R. Quintero-Bermudez, R. P. Sabatini, M. Lejay, O. Voznyy and E. H. Sargent, *ACS Nano*, 2017, **11**, 12378–12384.

92   T. T. Ngo, S. Masi, P. F. Mendez, M. Kazes, D. Oron and I. M. Seró, *Nanoscale Adv.*, 2019, **1**, 4109–4118.

93   T. T. Ngo and I. Mora-Seró, *J. Phys. Chem. Lett.*, 2019, **10**, 1099–1108.

94   R. C. Page, D. Espinobarro-Velazquez, M. A. Leontiadou, C. Smith, E. A. Lewis, S. J. Haigh, C. Li, H. Radtke, A. Pengpad, F. Bondino, E. Magnano, I. Pis, W. R. Flavell, P. O'Brien and D. J. Binks, *Small*, 2014, **11**, 1548–1554.

95   G. H. Carey, A. L. Abdelhady, Z. Ning, S. M. Thon, O. M. Bakr and E. H. Sargent, *Chem. Rev.*, 2015, **115**, 12732–12763.

96   E. J. D. Klem, H. Shukla, S. Hinds, D. D. MacNeil, L. Levina and E. H. Sargent, *Appl. Phys. Lett.*, 2008, **92**, 212105.

97   E. Sargent, *Nat. Photonics*, 2012, **6**, 133–135.

98   X. Lan, S. Masala and E. H. Sargent, *Nat. Mater.*, 2014, **13**, 233–240.

99   A. M. Goodman, *J. Appl. Phys.*, 1961, **32**, 2550–2552.

100   A. Henning, G. Günzburger, R. Jöhr, Y. Rosenwaks, B. Bozic-Weber, C. E. Housecroft, E. C. Constable, E. Meyer and T. Glatzel, *Beilstein J. Nanotechnol.*, 2013, **4**, 418–428.

101   B. F. Spencer, M. J. Cliffe, D. M. Graham, S. J. O. Hardman, E. A. Seddon, K. L. Syres, A. G. Thomas, F. Sirotti, M. G. Silly, J. Akhtar, P. O'Brien, S. M. Fairclough, J. M. Smith, S. Chattopadhyay and W. R. Flavell, *Surf. Sci.*, 2015, **641**, 320–325.

102   L. Kronik and Y. Shapira, *J. Vac. Sci. Technol. A Vacuum, Surfaces, Film.*, 1993, **11**, 3081.

103   P. A. Cox, *The Electronic Structure and Chemistry of Solids*, Oxford University Press, Oxford, 1987.

104   D. D. W. Grinolds, P. R. Brown, D. K. Harris, V. Bulovic and M. G. Bawendi, *Nano Lett.*, 2015, **15**, 21–26.

105   B. T. Diroll, E. A. Gaulding, C. R. Kagan and C. B. Murray, *Chem. Mater.*, 2015, **27**, 6463–6469.

106   I. Angeloni, W. Raja, R. Brescia, A. Polovitsyn, F. De Donato, M. Canepa, G. Bertoni, R. Proietti Zaccaria and I. Moreels, *ACS Photonics*, 2016, **3**, 58–67.

107   Z. Zhang, Y. T. Thung, X. Chen, L. Wang, W. Fan, L. Ding and H. Sun, *J. Phys. Chem. Lett.*, 2021, **12**, 191–198.

108   D. Zhitomirsky, O. Voznyy, L. Levina, S. Hoogland, K. W. Kemp, A. H. Ip, S. M. Thon and E. H. Sargent, *Nat. Commun.*, 2014, **5**, 3803.

109   J. Tang, *Materials Engineering for Stable and Efficient PbS Colloidal Quantum Dot*, PhD Thesis, University of Toronto, 2010.

110   P. N. Goswami, D. Mandal and A. K. Rath, *Nanoscale*, 2017, 1072–1080.

111   S. Yang, Z. Song, N. Gao, Z. Hu, L. Zhou, J. Liu, B. Zhang, G. Zhang, S. Jiang, H. Y. Li and H. Liu, *Sensors Actuators, B Chem.*, 2019, **286**, 22–31.

112   E. Beyreuther, J. Becherer, A. Thiessen, S. Grafstr and L. M. Eng, *Surf. Sci.*, 2013, **612**, Pages 1-9.

113   R. Saran and R. J. Curry, *Nat. Photonics*, 2016, **10**, 81–92.

114   D. Bozyigit, S. Volk, O. Yarema and V. Wood, *Nano Lett.*, 2013, **13**, 5284–5288.

115   A. A. Bessonov, M. Allen, Y. Liu, S. Malik, J. Bottomley, A. Rushton, I. Medina-Salazar, M. Voutilainen, S. Kallioinen, A. Colli, C. Bower, P. Andrew and T. Ryhänen, *ACS Nano*, 2017, **11**, 5547–5557.

116   S. Baek, S. Lee, J. H. Song, C. Kim, Y. Ha, H. Shin, H. Kim, S. Jeong and J. Lee, *Energy Environ. Sci.*, 2018, **11**, 2078–2084.

117   B. Martín-García, Y. Bi, M. Prato, D. Spirito, R. Krahne, G. Konstantatos and I. Moreels, *Sol. Energy Mater. Sol. Cells*, 2018, **183**, 1–7.

118   D. Zherebetskyy, M. Scheele, Y. Zhang, N. Bronstein, C. Thompson, D. Britt, M. Salmeron, P. Alivisatos and L.-W. Wang, *Science*, 2014, **344**, 1380–1384.

119   Y. Zhang, D. Zherebetskyy, N. D. Bronstein, S. Barja, L. Lichtenstein, A. P. Alivisatos, L. W. Wang and M. Salmeron, *ACS Nano*, 2015, **9**, 10445–10452.

120   M. Albaladejo-Siguan, D. Becker-Koch, A. D. Taylor, Q. Sun, V. Lami, P. Goldberg Oppenheimer, F. Paulus and Y. Vaynzof, *ACS Nano*, 2019, **14**, 384–393.

121   H. Heinemann, G. A. Somorjaf and B. Marchon, 1988, **26**, 507–514.

122   M.-J. Choi, J. Oh, J.-K. Yoo, J. Choi, D. M. Sim and Y. S. Jung, *Energy Environ. Sci.*, 2014, **7**, 3052.

123   C. T. Smith, M. A. Leontiadou, P. C. J. Clark, C. Lydon, N. Savjani, B. F. Spencer, W. R. Flavell, P. O'Brien and D. J. Binks, *J. Phys. Chem. C*, 2017, **121**, 2099–2107.

124   A. Bakulin, S. Neutzner, H. J. Bakker, L. Ottaviani, D. Barakel and Z. Chen, *ACS Nano*, 2013, **7**, 8771–8779.

125   S. Kahmann, M. Sytnyk, N. Schrenker, G. J. Matt, E. Spiecker, W. Heiss, C. J. Brabec and M. A. Loi, *Adv. Electron. Mater.*, 2018, **4**, 1700348.

126   H. Lu, J. Joy, R. L. Gaspar, S. E. Bradforth and R. L. Brutchey, *Chem. Mater.*, 2016, **28**, 1897–1906.

127   M. Biondi, M. J. Choi, S. Lee, K. Bertens, M. Wei, A. R. Kirmani, G. Lee, H. T. Kung, L. J. Richter, S. Hoogland, Z. H. Lu, F. P. García De Arquer and E. H. Sargent, *ACS Energy Lett.*, 2021, **6**, 468–476.

128   S. Kahmann and M. A. Loi, *Appl. Phys. Rev.*, 2020, **7**, 041305.

129   J. J. Choi, J. Luria, B. R. Hyun, A. C. Bartnik, L. Sun, Y. F. Lim, J. A. Marohn, F. W. Wise and T. Hanrath, *Nano Lett.*, 2010, **10**, 1805–1811.

130   S. W. Clark, J. M. Harbold and F. W. Wise, *J. Phys. Chem. C*, 2007, **111**, 7302–7305.

131   S. Liu, C. Zhang, S. Li, Y. Xia, K. Wang, K. Xiong, H. Tang, L. Lian, X. Liu, M. Y. Li, M. Tan, L. Gao, G. Niu, H. Liu, H. Song, D. Zhang, J. Gao, X. Lan, K. Wang, X. W. Sun, Y. Yang, J. Tang and J. Zhang, *Adv. Funct. Mater.*, 2021, **31**, 2006864.

132   M. C. Weidman, K. G. Yager and W. A. Tisdale, *Chem. Mater.*, 2015, **27**, 474–482.

133   C. B. Murray and C. R. Kagan, *Annu. Rev. Mater. Sci.*, 2000, **30**, 545–610.

134   H. R. You, J. Y. Park, D. H. Lee, Y. Kim and J. Choi, *Appl. Sci.*, 2020, **10**, 975.

135   X. Jin, W. Sun, Z. Chen, T.-H. Wei, C. Chen, X. He, Y. Yuan, Y. Li and Q. Li, *ACS Appl. Mater. interfaces*, 2014, **6**, 8771–8781.

136   D. C. Lee, I. Robel, J. M. Pietryga and V. I. Klimov, *J. Am. Chem. Soc.*, 2010, **132**, 9960–9962.

137   G. Konstantatos, M. Badioli, L. Gaudreau, J. Osmond, M. Bernechea, F. P. G. De Arquer, F. Gatti and F. H. L. Koppens, *Nat. Nanotechnol.*, 2012, **7**, 363–368.

138   A. B. Greytak and M. V. S. Chandrashekhar, *ACS Appl. Electron. Mater.*, 2019, **2**, 134–139.

139   C. Busche, L. Vilà-Nadal, J. Yan, H. N. Miras, D. L. Long, V. P. Georgiev, A. Asenov, R. H. Pedersen, N. Gadegaard, M. M. Mirza, D. J. Paul, J. M. Poblet and L. Cronin, *Nature*, 2014, **515**, 545–549.

140   S. Xu, D. Thian, S. Wang, Y. Wang and F. B. Prinz, *Phys. Rev. B*, 2014, **90**, 144202.

141   L. Qu, D. Unruh and G. T. Zimanyi, *Phys. Rev. B*, 2021, **103**, 195303.

142   H. Lepage, A. Kaminski-Cachopo, A. Poncet and G. Le Carval, *J. Phys. Chem. C*, 2012, **116**, 10873–10880.

143   L. Hu, S. Huang, R. Patterson and J. E. Halpert, *J. Mater. Chem. C*, 2019, **7**, 4497–4502.